Actin Polymerization upon Processive Capping by Formin: A Model for Slowing and Acceleration

Tom Shemesh and Michael M. Kozlov
Department of Physiology and Pharmacology, Sackler Faculty of Medicine, Tel Aviv University, Tel Aviv, Israel

ABSTRACT Formin family proteins act as processive cappers of actin filaments, and determine the dynamics of a number of intracellular processes that are based on actin polymerization. The rate of filament growth upon processive capping varies within a broad range depending on the formin type and presence of profilin. While FH2 domains of various formins slow down polymerization by different extents, the FH1-FH2 domains in conjunction with profilin accelerate the reaction. Study of the physical mechanism of processive capping is vital for understanding the intracellular actin dynamics. We propose a model predicting that variation of a single physical parameter—the effective elastic energy of the formin-capped barbed end—results in the observed diversity of the polymerization rates. The model accounts for the whole range of the experimental results including the drastic slowing down of polymerization by FH2 of Cdc12 formin and the 4.5-fold acceleration of the reaction by FH1-FH2 of mDai1 formin in the presence of profilin. Fitting the theoretical predictions to the experimental curves provides the values of the effective elastic energies of different formin-barbed end complexes.

INTRODUCTION

Formin family proteins regulate actin assembly in many cell types (1–6). Formins have been implicated in formation of actin cables in yeast and cytokinetic contractile rings, actin filament formation within filopodia, and initiation of actin polymerization in focal adhesions, and adherence junctions between cells (7–16). All formins are characterized by the highly conserved formin homology-2 (FH2) domain, and the proline-rich formin homology-1 (FH1) domain. FH2 is responsible for formin interaction with actin (17), whereas FH1 binds formin to regulating proteins, such as profilin (7).

Formins are able to play a dual role in actin polymerization: they nucleate actin filament self-assembly, and also cap the barbed ends of the growing filaments by remaining bound to them. While serving as a capper, formin enables addition of new actin monomers to the barbed end. The latter phenomenon, which is the focus of the present work, is called processive capping (18). The physiological role of the processive capping is to protect the barbed ends from capping by other proteins, and hence to prevent interruption of polymerization and enable a continuous growth of long linear filaments. To effectively fulfill this task, the processive capping has to keep the thermodynamic and kinetic characteristics of the polymerization process similar to those of uncapped barbed ends. Attempts to understand the physical mechanism of processive capping motivated a series of recent experimental and theoretical studies (19–22).

The thermodynamics of barbed end polymerization are characterized by the critical concentration, which is unaffected by processive capping (23). Physics of this phenomenon has been accounted for by the elastic model of processive capping (24).

Kinetically, actin polymerization proved to be strongly influenced by the type and structure of the participating formins (25). The minimal unit necessary for performing the processive capping is an FH2 homodimer (see for review (1,2)). While the FH2 dimers of all formins reduced the filament elongation rate, the extent of this effect varied from practically complete polymerization stop for Cdc12 formin to an almost unaltered polymerization rate for mDia1 formin (25). Similar effects were produced by cappers consisting of FH1-FH2 domains of different formins in the absence of profilin (25). In contrast, addition of profilin converted the slowing down to an acceleration of polymerization. In the presence of profilin, the elongation rate of filaments capped by FH1-FH2 domains of Cdc12 was close to that of uncapped formin, while the FH1-FH2 domain of mDia1 speeded up polymerization by a factor of 4.5 (25). ATP hydrolysis by mDia1 FH1-FH2 domain coupled to profilin-actin polymerization was observed to accelerate filament growth by even more ((20), but see (25)).

Here we present a unifying mechanism of actin polymerization and depolymerization upon processive capping by FH2 and FH1-FH2 domains of different formins in the absence and presence of profilin. This mechanism accounts for the whole range of the experimentally observed rates of filament elongation, including the nearly fivefold acceleration. According to our model, the single physical property of the system controlling the polymerization-depolymerization rate is the energy of the formin-barbed end complex, U_F, which consists of the effective elastic energy of the mutual formin-actin deformation, and the formin-barbed end interaction energy. The energy U_F is suggested to vary between different formin types, most probably due to different formin rigidities, and to be influenced by profilin. Fitting the model

Submitted September 29, 2006, and accepted for publication November 16, 2006.

Address reprint requests to Michael M. Kozlov, Tel.: 972-3-640-7863; E-mail: michk@post.tau.ac.il.

0006-3495/07/03/1512/10 $2.00

doi: 10.1529/biophysj.106.098459

predictions to the experimental results provides U_F of different formin-barbed end complexes with and without profilin.

Description of the system

An FH2 dimer consists of two identical structural units called bridges, which are connected to each other by flexible tethers to form a closed ring (26). There are two suggested states of binding of this ring to the barbed end of an actin filament: the ''blocked'' and the ''open'' states (26). In the blocked state, the FH2 dimer is attached in all its binding sites to the three terminal actin subunits of the actin filament so that addition of new actin monomers is sterically prevented (Fig. 1 *a*). In the open-state, the FH2 ring is shifted toward the filament end, bound to only two terminal actin subunits, and exposes one vacant binding site to allow attachment of a new actin monomer (Fig. 1 *b*). Addition of an actin monomer to the barbed end, which constitutes a polymerization step, transforms the open state into the blocked one. Preparation of the system to the next polymerization step requires transition from the newly formed blocked state to the open state by further shifting of the formin dimer toward the filament end and partial detachment of one of its bridges. This completes one cycle of transformations of the formin-barbed end complex accompanying the polymerization process.

Depolymerization also implies repetitive transitions between the open and blocked states of the FH2-barbed end complex, but in the opposite sequence. Importantly, detachment of the ultimate actin subunit during a depolymerization step must occur from the blocked rather than the open state (26).

The previous models (24,26,27) suggested that the blocked-to-open state transition is driven by the release of elastic energy, which is built up within the blocked state of the FH2-actin complex and relaxes in the open state. This is based on the observed deformations of the filament barbed end and the FH2 dimer upon formation of the formin-barbed end complex (26). The periodic accumulation and relaxation of the elastic energy is essential for the model presented here.

Statement of the problem

Our goal is to analyze theoretically the kinetics of actin polymerization-depolymerization upon processive capping, based on the structural knowledge of the formin-barbed end complex summarized above. This requires modeling the transitions between the open and blocked states of the system, taking into account the whole range of intermediate states between the open and blocked states, and the transitions between them.

Our further aim is to compare the kinetics of actin polymerization upon processive capping with those of uncapped actin, and use the parameters known for the latter system for quantification of the processive capping model. To this end, polymerization of uncapped barbed ends has to be treated by the same model as that accounting for processive capping, with vanishing values of parameters describing the effects of the formin cap.

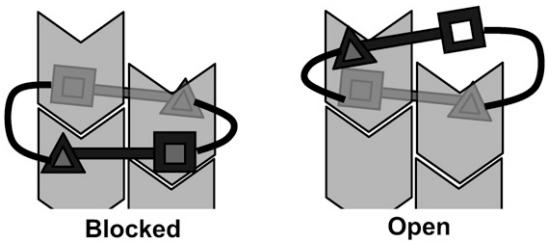

FIGURE 1 Open and blocked states of the formin-barbed end complex according to Otomo et al. (26).

THE MODEL

Polymerization cycle of formin-capped barbed end

We consider the barbed end polymerization as consisting of two sequential subprocesses: transition of the formin-barbed end complex between the blocked and the open states (Fig. 2 *a*), and addition of a new monomer from the solution to the barbed end (Fig. 2 *b*). Generally, there are two alternative ways to describe these subprocesses—discretely by Markov chain approach or continuously by Fokker-Planck formalism (28). While recognizing the relative advantages and disadvantages of each of the approaches in relation to our system, we will use the continuous description since, according to the structural data (26), the binding sites between actin subunits and the formin bridges are extended along the protein interface rather than pointlike. Hence, within the continuous approach, we characterize the subprocesses by the effective reaction coordinates x and y, respectively. Since the opening-closing of the formin-barbed end complex includes movement

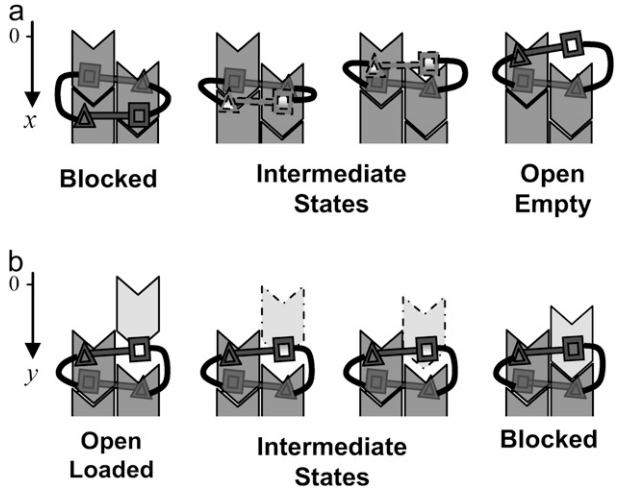

FIGURE 2 Continuous subprocesses of the polymerization cycle. (*a*) Transition of the formin-barbed end complex between the blocked and open states. (*b*) Addition of a new actin monomer to the barbed end.

of the formin dimer (Fig. 2 *a*), and the new monomer addition can be characterized by its position with respect to the terminal subunits of the barbed end (Fig. 2 *b*), the two reaction coordinates, x and y, have the meaning and dimension of length.

We consider the polymerization cycle illustrated by a scheme in Fig. 3 *a*. The process begins with establishment of a preliminary bond between a new actin monomer and the barbed end. This can happen only when the formin-barbed end complex is completely open ($x = 0$), the corresponding state of the system referred to as the open-empty state, which is illustrated in Fig. 2 *a*, and by the lower vertex of the scheme in Fig. 3 *a*. The preliminary binding of a new monomer creates the state referred to below as the open-loaded state illustrated in Fig. 2 *b*, and by the upper vertex of the scheme in Fig. 3 *a*. This is followed by a continuous attachment stage during which the monomer moves from the preliminarily bound ($y = 0$) position toward the fully bound ($y = y_0$) position (Fig. 2 *b*), as illustrated by the upper arrow in Fig. 3 *a*. The resulting state is the blocked state corresponding to the middle vertex of the scheme (see Fig. 3 *a*).

The next subprocess, illustrated by the lower arrow of Fig. 3 *a*, consists of a continuous transition of the formin-barbed end complex from the blocked ($x = x_0$) to the open-empty state ($x = 0$) state (Fig. 2 *a*), thereby completing the polymerization cycle. Note that the blocked state is common for the two sequential subprocesses and corresponds to $y = y_0$ on one hand, and $x = x_0$, on the other.

The process of depolymerization consists of the same subprocesses but oppositely directed (*counterclockwise* along the scheme; see Fig. 3 *a*). The formin-barbed end complex undergoes a continuous transformation from the open-empty to the blocked state. This is followed by a continuous monomer transition from the fully to preliminarily bound position, which brings the system from the blocked to the open-loaded state. The last stage is the breakage of the preliminary bond in the open-loaded state, and release of the actin monomer into the surrounding solution, which completes the depolymerization step and creates the open-empty state again.

Importantly, formation and breakage of the preliminary bond is allowed only in the open-empty and open-loaded states, respectively, and are forbidden in the blocked and all the intermediate states of the system. Note, however, that the open-empty and open-loaded states might be composed, in their turn, of a variable range of substates (see below and in the Appendix).

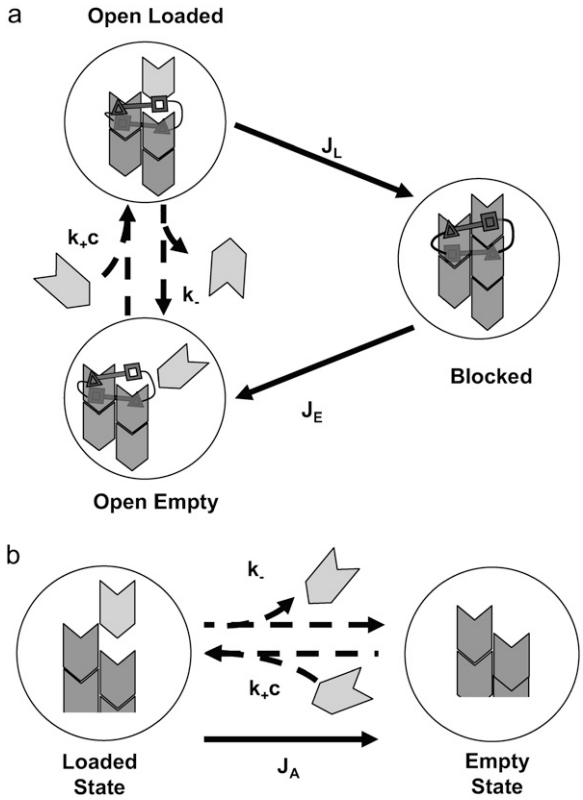

FIGURE 3 Schematic illustration of the polymerization cycle. Arrows marked by J_L, J_E, and J_A indicate time-averaged fluxes during steady-state polymerization. Reversing those arrows would depict steady-state depolymerization cycles (*a*). Polymerization of formin-capped barbed end. (*b*) Polymerization of uncapped formin.

Polymerization cycle of uncapped barbed end

Polymerization (depolymerization) of uncapped actin consists of just one subprocess of a new actin monomer addition (detachment) (Fig. 3 *b*). In this case, there is no blocked state of the system; nevertheless, we define, for the sake of convenience, the empty and loaded states of this system. In the empty state illustrated in the right panel of Fig. 3 *b*, the barbed end is ready for absorbing a new actin monomer. The loaded state forms when a new actin monomer establishes a preliminary bond with the barbed end, as illustrated by the left panel of Fig. 3 *a*. We suggest that a polymerization cycle begins with a discrete step of forming a preliminary bond between an actin monomer and the barbed end in its empty state. As a result, the system transits form the empty to the loaded state (Fig. 3 *b*). This is followed by a continuous process of attachment of the actin monomer to the barbed end, which results in a transition from the loaded to the empty state again (Fig. 3 *b*).

Note that division of the binding process into a discrete step followed by a continuous one rather than treating the binding process as a single event, is in fact a necessary generalization, needed to take into account the internal properties of the system that affect the overall elongation rates. The polymerization cycle is illustrated by the scheme in Fig. 3 *b* and is characterized by the reaction coordinate z varying between 0 for the loaded and z_0 for the empty state.

Essentially, we assume that despite the absence of formin, a new actin monomer can start the attachment process only when the barbed end is in the empty state. This condition

may be restated as the requirement that a monomer must complete its process of attachment to the filament, before another monomer may begin to bind. In the course of depolymerization, detachment of actin monomers proceeds only from the loaded state, with the mechanistic interpretation that monomers may begin unbinding from the filament only when the preceding monomers have become fully detached. The monomer attachment (detachment) cannot occur to (from) the intermediate states of the system.

Energies

Each subprocess of the kinetic schemes (Fig. 3, *a* and *b*) is related to changes of free energy. For the sake of simplicity, we will refer to the free energy as the energy.

The energy released at the stage of the preliminary bond formation between the new actin monomer and the barbed end will be denoted by U_{AA}^{prel}. We assume that this stage does not include any actin-formin interaction. Hence, the related energy U_{AA}^{prel} originates from the actin-actin interaction only and characterizes both the formin-capped and uncapped barbed ends (see Discussion for further treatment of model's assumptions).

The intermediate states the system goes through in the course of the two continuous subprocesses of transition between the open and blocked states (Fig. 3 *a*) are characterized by the elastic energy of the formin-barbed end complex, u_{el}, the actin-formin interaction energy, u_{AF}, and the actin-actin interaction energy, u_{AA}. All these energies are assumed to vary continuously along the effective reaction coordinates x and y for the open-empty-to-blocked and open-loaded-to-blocked transition, respectively.

Continuous attachment of an actin monomer to the uncapped barbed end (Fig. 3 *b*) is characterized by the actin-actin interaction energy u_{AA}, which depends on the reaction coordinate z.

The total energy of an intermediate state of the actin monomer attachment (Fig. 2 *b*) in the course of the open-loaded-to-blocked transition consists of all three contributions, $u_{el}(y) + u_{AF}(y) + u_{AA}(y)$. The total energy of the intermediate states of the open-empty-to-blocked transition (Fig. 2 *a*) includes only two contributions, $u_{el}(x) + u_{AF}(x)$, because no actin-actin interaction is involved in this subprocess. We denote the sum of the two energy contributions related to formin as the effective formin energy, $u_F = u_{el} + u_{AF}$. Using this notation, the intermediate state energies of the two subprocesses are $u_F(y) + u_{AA}(y)$, and $u_F(x)$, respectively.

For the following, we introduce the notations for the total energy changes resulting from each of the subprocesses. The total change of the formin energy is equal for the two subprocesses and is denoted by U_F,

$$U_F = u_F(x_0) - u_F(0) = u_F(y_0) - u_F(0). \quad (1)$$

The total change of the actin-actin interaction energy resulting from the continuous stage of the new monomer attachment is $U_{AA}^{cont} = u_{AA}(y_0) - u_{AA}(0)$. The total actin-actin interaction energy released after both the preliminary and the continuous stages of actin attachment is denoted by $U_{AA}^{tot} = U_{AA}^{prel} + U_{AA}^{cont}$.

Polymerization of an uncapped filament is described only by the actin-barbed end interaction energies of the preliminary (U_{AA}^{prel}) and the continuous ($u_{AA}(z)$) stages. The corresponding total energy changes, U_{AA}^{cont} and U_{AA}^{tot}, are the same as for the formin-capped filament.

Recall that all the energies introduced in this section have a meaning of free energies, which include contributions of both internal energy and entropy. Depending on the process, the energy change can be determined by enthalpy, entropy, or a combination of the two. For example, the polymerization energy of uncapped actin, U_{AA}^{tot}, has been shown to have an entropic rather than enthalpic origin (29,30).

Strategy of analysis and main equations

Formin-capped filament

The goal of the work is to calculate the filament polymerization rate R_{AF}. The approach we are using is based on probabilities of different states of the system and the related probability fluxes, which describe the system progression along the substages of the polymerization cycle (Fig. 3 *a*). The meaning of the probability flux through a certain state is the probability of the system to transition via this state in a given direction in unit time. The polymerization rate, R_{AF}, is identical to the probability flux from the open-empty to the open-loaded state of the system.

We denote by $\rho_E(x)$ the probability density of the intermediate states in the continuous range between the blocked and the open-empty states (Fig. 2 *a*); and by $\rho_L(y)$ the probability density for the range of intermediate states corresponding to continuous attachment of a new actin monomer to the barbed end (Fig. 2 *b*).

The probabilities of the open-empty and open-loaded states, which are the discretely defined extremes of the two continuous ranges of intermediate states, are given by

$$\rho_E(0)\lambda \quad \text{and} \quad \rho_L(0)\lambda, \quad (2)$$

respectively. The coefficient λ represents a distance along the reaction coordinate that separates two adjacent states if the latter are described discretely rather than continuously.

In the blocked state, which is common for the two ranges of the intermediate states, the two probability densities must coincide:

$$\rho_E(x_0) = \rho_L(y_0). \quad (3)$$

The polymerization cycle includes three probability fluxes (Fig. 3 *a*).

The probability flux from the open-empty to the open-loaded state, J_{in}, determines, as mentioned above, the polymerization rate, $R_{AF} = J_{in}$. Accounting for Eq. 2, this flux can be expressed as

$$J_{in} = k_+ c\rho_E(0) - k_-\rho_L(0), \quad (4)$$

where k_+c is the rate of the preliminary bond formation between an actin monomer and the barbed end in the open-empty state, c being the bulk concentration of actin monomers next to the barbed end; and k_- is the rate of the breakage of the preliminary bond in the open-loaded state. Note that, within our definitions, the rates k_+c and k_- include the length λ (Eq. 2) and, therefore, have units of length over time.

The second probability flux, J_L, corresponds to transition from the open-loaded to the blocked state of the system, and the third probability flux, J_E, describes evolution of the formin-barbed end complex from the blocked to the open-empty state (the *upper* and *lower arrows* in the scheme in Fig. 3 *a*). Taking into account the energies of the intermediate states defined above, and using the Fokker-Planck expressions, these two probability fluxes are given by

$$J_L = -D_L\frac{\partial\rho_L(y)}{\partial y} - \frac{D_L}{k_BT}\rho_L(y)\frac{\partial(u_F(y) + u_{AA}(y))}{\partial y}, \quad (5)$$

$$J_E = D_E\frac{d\rho_E(x)}{dx} + \frac{D_E}{k_BT}\rho_E(x)\frac{du_F(x)}{dx}, \quad (6)$$

where D_L and D_E are the coefficients of the effective diffusion of the system along the reaction coordinates y and x, respectively.

We consider the steady state in which all the fluxes are constant and equal to each other:

$$J_{in} = J_L = J_E. \quad (7)$$

To find the polymerization rates upon processive capping, we have to solve the system of Eqs. 4–7 accounting for Eq. 3.

Uncapped filament

The analysis in this case is a reduced version of that described above. The intermediate states of the system are described by the probability density $\rho_A(z)$, while the probabilities of the loaded and empty states are given, respectively, by $\rho_A(0)\cdot\lambda$ and $\rho_A(z_0)\cdot\lambda$. The probability flux J_{in} can be expressed as

$$J_{in} = k_+ c\rho_A(z_0) - k_-\rho_A(0). \quad (8)$$

The probability flux of continuous attachment of a monomer to the barbed end is given by

$$J_A = -D_A\frac{d\rho_A(z)}{dz} - \frac{D_A}{k_BT}\rho_A(z)\frac{du_{AA}(z)}{dz}, \quad (9)$$

where D_A is coefficient of the effective diffusion of the system along the reaction coordinate z.

We assume that the rate constants k_+c and k_- are equal to those in the presence of the formin cap. This is another manifestation of the assumption that the preliminary bond is identical in capped and uncapped systems (see Discussion). We adopt this assumption to focus on the effects of the elasticity of the formin-actin complex on the polymerization rate. Accounting for possible variations in these rate constants produced by formin leads to changes in the polymerization rate, which are additional to those predicted by our model. As discussed below, such variations have been addressed by the recent model of processive capping by formin in the presence of profilin (21).

Upon steady-state polymerization,

$$J_{in} = J_A. \quad (10)$$

Simultaneous solution of Eqs. 8 and 9 gives the polymerization rate, $R_{AA} = J_{in}$, of uncapped actin filaments.

RESULTS

Expressions for polymerization rates

The analytical results for the probability distributions, fluxes and, finally, the polymerization rates characterizing the actin filament assembly with, and in the absence of, processive capping are presented in the Appendix. In this section, we discuss the experimentally testable predictions of the model on the polymerization rates.

The polymerization rates of formin-capped, R_{AF}, and uncapped, R_{AA}, barbed ends are expressed, respectively, by Eqs. A10 and A3 through the bulk concentration of actin monomers in the solution, c, and the energy functions $u_F(\xi)$ and $u_{AA}(\xi)$ (where ξ denotes the reaction coordinate x, y, or z, depending on the subprocess). According to Eqs. A10, A3, and Eq. 1, both R_{AF} and R_{AA} vanish if the actin concentration has the critical value of

$$c = c^* = \frac{k_-}{k_+}e^{\frac{U_{AA}^{cont}}{k_BT}}, \quad (11)$$

where $k_BT \approx 0.6$ kcal/mol is the product of the Boltzmann constant and the absolute temperature.

The elongation rates are positive, $R_{AF} > 0$, $R_{AA} > 0$, corresponding to polymerization, if the actin concentration exceeds the critical value, $c > c^*$, and negative, $R_{AF} < 0$, $R_{AA} < 0$, meaning depolymerization, for $c < c^*$.

According to the general expressions (Eqs. A10 and A3), the polymerization rates, R_{AF} and R_{AA}, are nonlinear functions of the actin concentration and exhibit saturation beginning from certain c. On the other hand, the experimentally measured polymerization rates of both uncapped and formin-capped actin filaments (25,31) exhibit an effectively linear dependence on c in the range between $c^* \approx 0.1$ μM and at least 10 μM. Requirement of a quasi-linear dependence of R_{AF} and R_{AA} on c in the relevant concentration range will be the major criterion for determination of the system parameters below. Once this requirement is fulfilled, the polymerization rates R_{AF} and R_{AA} (Eqs. A3 and A10) can be expressed in this concentration range by simplified linear expressions $R_{AF} = \alpha_{AF}(c–c^*)$ and $R_{AA} = \alpha_{AA}(c–c^*)$. The filament assembly is then characterized by the elongation slopes α_{AF} and α_{AA}, which can be calculated numerically from Eqs. A10 and A3, respectively.

To express the polymerization rates in analytical form, we treat the formin energy profile, u_F, and the energy profile of actin-actin interaction, u_{AA}, as linear functions of the reaction

coordinates: $u_F(\xi) = U_F \cdot \frac{\xi}{\xi_0}$, $u_{AA}(\xi) = U_{AA} \cdot \frac{\xi}{\xi_0}$. This means that both the formin energy and the energy of actin-actin interaction are accumulated (or released) gradually in the course of the continuous stages. (To ensure the robustness of the model conclusions we analyzed numerically also some nonlinear energy profiles; see Discussion.) The resulting expressions for the elongation slopes of the formin-capped and uncapped filaments are given by Eqs. A11 and A5, respectively. They are determined by the following system parameters: the total energy changes U_F and U_{AA}; the rate constants k_+ and k_-; the effective diffusion coefficients, D_E, D_L, and D_A; and the ranges of the reaction coordinates x_0, y_0, and z_0.

Elongation rates

To analyze the elongation rates predicted by the model, we assume all the diffusion coefficients to equal that of actin monomers in water, $D_E = D_L = D_A = 5 \cdot 10^7$ nm^2/s (see Discussion for sensitivity of the results to this assumption). The ranges of the reaction coordinates can be estimated as the half size of an actin monomer $x_0 = y_0 = z_0 \approx 2.8$ nm, which is the average distance of movement of a formin dimer in the stair-stepping model (24,26,27) and of shifting of a new actin subunit along the barbed end before reaching its final position (Fig. 2). Three other parameters, U_{AA}, k_+, and k_-, are interconnected by Eq. 11 via the known value of the critical concentration $c^* = 0.1$ μM (32). Using Eq. 11 to express k_-, we are left with three free parameters: the total change of the formin energy U_F, the total change of the actin-actin energy resulting from the continuous attachment stage, U_{AA}, and the rate of generation of the preliminary bond, k_+.

We first analyze the model prediction for polymerization rate of uncapped actin, R_{AA}. Inserting the value of the elongation slope, α_{AA}, measured in Kovar et al. (25) into Eq. A5, we obtain the relationship between k_+ and U_{AA} (Eq. A6), denoted as $k_+^{fit}(U_{AA})$, which fits the experimental results for uncapped actin (25).

We use the found relationship $k_+^{fit}(U_{AA})$ to examine the rate of polymerization upon processive capping, R_{AF}, for different values of the two remaining free parameters, U_{AA} and U_F. The elongation slope α_{AF} depends on the energies U_{AA} and U_F according to Eq. A12 accounting for Eq. A6. This dependence is illustrated by the ridgelike surface in Fig. 4 *a* and represents the main result of this work. For comparison, the elongation slope of uncapped actin α_{AA} is presented in the same figure by a flat surface.

The Fig. 4 *a* shows that for any value of U_{AA}, the elongation slope α_{AF} varies considerably with the total formin energy U_F. Whereas U_{AA} is determined by the actin-actin interactions only, U_F accounts for the properties of the formin-barbed end complex and, therefore, must vary for different formin types in agreement with the experimental observations. Hence, the elongation rate depends strongly on the formin type. Importantly, according to Fig. 4 *a*, the elongation slope of formin-capped filaments, α_{AF}, can be smaller or larger than that of the uncapped formin, α_{AA}, depending on the energies U_{AA} and U_F. This means that the processive capping is predicted to be able to both slow down and accelerate polymerization depending on the properties of the formin-barbed complex accounted for by the formin energy U_F. Thus, our model predicts a possibility of both slowing down and acceleration of the filament elongation by processive capping in the absence of any additional energy input such as that of ATP hydrolysis.

Further, for any U_{AA}, the elongation slope α_{AF} changes nonmonotonously with the total formin energy U_F, and there is an optimal U_F that results in a largest elongation rate of the filament. The largest values of α_{AF} are lying along the crest of

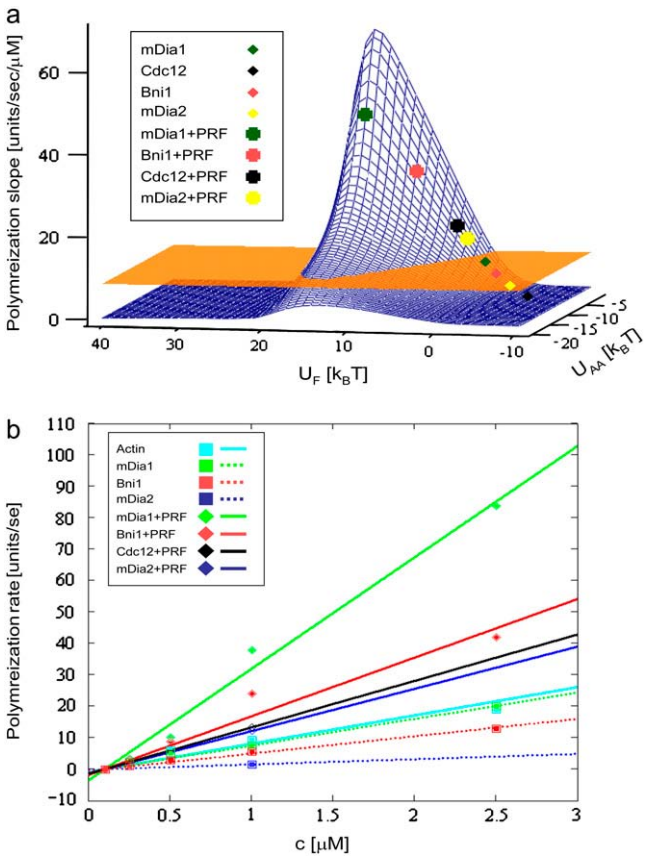

FIGURE 4 Kinetic characteristics of the polymerization process. Comparison with the experimental results from Kovar et al. (25). (*a*) Elongation slope as a function of the total formin energy U_F and the total energy interaction of actin monomer and the barbed end released as a result of the continuous stage of the monomer addition, U_{AA}. The ridgelike surface represents polymerization kinetics of the formin-capped barbed end. The flat surface describes polymerization of uncapped barbed end. The points correspond to polymerization rates of different formins with and without profilin as explored experimentally in Kovar et al. (25). The fitting procedure is described in the main text. (*b*) Elongation rate as a function of actin monomer concentration for different values of the total formin energy, U_F. The points correspond to the experimental results of Kovar et al. (25). The values of the formin energy U_F fitted to describe the polymerization kinetics of different formins (25) are: 0 k_BT for mDia2(FH1FH2); 2.5 k_BT for Bni1(FH1FH2); 4 k_BT for mDai1(FH1FH2); 6 k_BT for mDia2(FH1FH2)+profilin; 6.5 k_BT for Cdc12(FH1FH2)+profilin; 8 k_BT for Bni1(FH1FH2)+profilin; and 16 k_BT for mDia1(FH1FH2)+profilin.

the ridgelike surface (Fig. 4 *a*). As U_{AA} increases, the corresponding largest elongation slope increases, and, at $U_{AA} \approx -15\ k_BT$ it exceeds the elongation slope of uncapped filaments. The maximal elongation slope is predicted for $U_{AA} \to 0$, and corresponds to greater than five times' acceleration of actin polymerization by processive capping compared to polymerization rate of uncapped filament (Fig. 4 *a*).

Comparison with experimental results

The present model can account for the whole range of actin polymerization rates observed in the presence of different formin domains with and without profilin. The largest polymerization rate, exceeding by a factor of ~4.5 that of uncapped actin, was measured for FH1-FH2 domain of mDia1 in the presence of profilin (25). We assume that the corresponding polymerization rate $\alpha_{AF} = 35.7\ s^{-1}\ \mu M^{-1}$ is described by a point on the crest of the ridgelike surface (Fig. 4 *a*) and obtain that, within this assumption, the system is described by $U_{AA} \approx -3\ k_BT$.

Due to the nonmonotonic dependence of α_{AF} on U_F (Fig. 4 *a*), the formin energies U_F of the other formin systems characterized by slower polymerization rates can be either larger or smaller than U_F of mDia1 in the presence of profilin. To choose between these two possibilities we use the requirement of the quasi-linear dependence of the polymerization rate R_{AF} on the actin concentration c in the range between 0 and 10 μM. Our numerical analysis of Eq. A10 shows that for larger U_F the dependence of R_{AF} on c considerably deviates from a linear one already at concentration below 1 μM, while for lower U_F this dependence looks linear up to actin concentrations exceeding 10 μM. Therefore, all other formins have to possess U_F smaller than that of mDia1 with profilin.

Using the measured values of the elongation slope for different formins represented by the experimental points in Fig. 4 *a*, we find the formin energy U_F corresponding to each formin system. This allows us to obtain a series of the actin concentration dependences for the polymerization rates, R_{AF}, corresponding to the whole pool of the experimental data (25), as illustrated in Fig. 4 *b*. The values of the total formin energy U_F describing the investigated formin systems are given in the legend of Fig. 4. Among them, the minimal formin energy $U_F \approx 0$ corresponds to the mDia2 (FH1H2) and the maximal $U_F \approx 16\ k_BT$ to mDia1(FH1FH2) in the presence of profilin. Estimations show that U_F of Cdc12 in the absence of profilin should be slightly negative, meaning that the negative energy of actin-formin interaction U_{AF} has an absolute value exceeding that of the elastic energy U_{el}.

DISCUSSION

Polymerization rate is controlled by the effective rigidity of formin

Formin-capped actin filaments exhibit a variety of elongation rates depending on the type of formin and the presence of profilin (20,25). Polymerization is slowed down by dimers of FH2 domains of various formins, and is accelerated by FH1-FH2 domains in the presence of profilin.

We have suggested a model predicting the observed diversity of polymerizations rates upon processive capping and explaining this effect by variation of only one system parameter—the total energy of the formin-barbed end complex, U_F, as illustrated in Fig. 4 *a*. This energy is the sum of the formin-actin binding energy, U_{AF}, and the elastic energy, U_{el}, of the mutual deformation of formin and the filament-barbed end. Both contributions and, particularly, the elastic energy U_{el}, which is determined by the effective rigidity of the formin-barbed end complex (24), can vary considerably between different formins. For example, variations in length of the tethers connecting the two FH2 bridges within the dimer (26) can influence the formin effective rigidity and, hence, U_{el}.

Acceleration of polymerization by profilin

The maximal polymerization rate upon processive capping is predicted by our model to be approximately five times larger than that of uncapped actin, R_{AA} (Fig. 4 *a*). This prediction is rather close to the maximal elongation rate observed experimentally for FH1-FH2 dimers of mDia1in the presence of profilin (25), which exceeds R_{AA} by a factor of 4.5. The more precise fitting presented in Results shows that the whole pool of the experimental results, including the 4.5-fold acceleration, can be explained assuming that the energy U_{AA} of the actin monomer-barbed end interaction corresponding to the continuous stage of the monomer attachment process is $U_{AA} = -3\ k_BT$. This is a relatively small part of the total energy of actin-actin interaction U_{AA}^{tot}, which includes, in addition to U_{AA}, the energy of the preliminary actin-actin bond U_{AA}^{prel}, and can be estimated based on the value of the critical concentration c^* as $U_{AA}^{tot} = k_BT\ln(c^*/c_W) \approx -20\,k_BT$ ($c_W \approx 55$ M being the water concentration) (24). Hence, the largest part of the total actin-actin energy should correspond to the preliminary bond $U_{AA}^{prel} \approx -17\,k_BT$.

The fitted values of the total formin energies U_F corresponding to the different formin systems are presented in the legend to Fig. 4. According to the fitting results, the energy U_F, is larger in the presence of profilin. This can be justified by reasoning that in the absence of profilin, only FH2 domain interacts with the polymerizing actin monomer and undergoes the related deformations. Profilin mediates binding of the new actin monomer to the FH1 domain (7). As a result, the FH1 domain should also undergo deformation in the course of the monomer addition to the barbed end. Consequently, the FH1 domain contributes its rigidity to the effective rigidity of the formin-barbed end complex and increases the elastic part of the energy U_F.

The previously suggested model for the acceleration of actin polymerization by profilin (21) proposes that profilin effectively increases the concentration of actin monomers near the barbed end by using the FH1 domain as a means of

exploring the space around the barbed end. Further, this model suggests that profilin assists in the orientation alignment of the monomers before their binding with the filament, which results in a greater on-rate of the monomer binding. These effects are complementary to those described by our model, and may be integrated into it by defining the effective values of the binding rate $k_+^{\text{eff}} > k_+$ and the actin monomer concentration $c^{\text{eff}} > c$, thereby accounting for the actin monomers orientation and accumulation, respectively.

Origin of the acceleration effect and the optimal rigidity

The increase of the polymerization rate by an elastic formin cap, which does not require energy input from an external source such as ATP hydrolysis, may appear counterintuitive. Yet, it has a rather simple physical origin.

The polymerization rate is determined by the probabilities of the system to be in the open-empty and the open-loaded states, which serve as gates for actin monomer attachment to and detachment from the barbed end (see Eqs. 4 and 8). In the blocked state and all the intermediate states, the system cannot exchange the monomers with the surrounding solution. The larger the overall probability of the system to be within the range of the intermediates states, the lower the chances to exchange monomers with the solution, and, hence, the more influenced is the polymerization rate.

For the formin-capped barbed end, the probabilities of different states are largely determined by the formin energy U_F. For small U_F, the system is effectively smeared within the broad continuous range of intermediate states corresponding to two subprocesses—attachment of the new monomer and opening of the formin-barbed end complex (movement of formin bridge). The probability of the open-empty state in this case is small and lesser than the corresponding probability for uncapped filament, where the range of intermediate states is limited by only one subprocess of the monomer attachment. Hence, the polymerization rate of formin-capped filament is lower than that of an uncapped filament. As U_F increases due to the growing formin rigidity, the intermediate states become more and more unfavorable. This increases the chances of the formin-capped barbed end to be in the open-empty state and boosts the actin monomer influx. In the parameter range discussed above, the resulting polymerization can exceeds that of an uncapped actin filament.

As the formin rigidity, and, hence, U_F, increases even further, progress of the system through the polymerization cycle (Fig. 3 *a*) requires overcoming of a growing energy barrier between the open-loaded and blocked states, which creates an effective bottleneck for the probability fluxes and reduces the overall polymerization rate. This results in nonmonotonous dependence of the polymerization rate on U_F at every fixed U_{AA}, as illustrated by the ridgelike surface (Fig. 4 *a*). According to Fig. 4 *a*, the formin energy corresponding to the largest polymerization rates is close to $U_F \approx 15\ k_BT$. The formin-actin binding energy can be estimated as $U_{AF} \approx -5\ k_BT$, which takes into account that, while the total binding energy is $\sim -20\ k_BT$ (24), the cycle of processive capping includes disruption and reconnection of only one out of four FH2-actin bonds. Hence, the maximal elongation rate requires the elastic energy of $U_{el} = U_F - U_{AF} \approx 20\ k_BT$. A similar estimation was obtained in Kozlov and Bershadsky (24) based on qualitative considerations, and the resulting rigidity of the formin-barbed end complex was shown to be comparable with the rigidity of actin filaments.

Model assumptions

Numerical predictions of the model illustrated in Fig. 4 are based on two assumptions. First, we used specific values of the effective diffusion coefficients $D_L = D_E = D_L = 5 \cdot 10^7$ nm^2/s and the ranges of the reaction coordinates $x_0 = y_0 = z_0 = 2.8$ nm. The predicted polymerization rates depend only on the combinations of these parameters having a meaning of diffusion times, $\tau_{\text{diff}} \approx \frac{x_0^2}{D_L} \approx \frac{y_0^2}{D_E} \approx \frac{z_0^2}{D_A} \approx 10^{-7}$s. These characteristic times are much smaller than the time of formation of the preliminary bond between an actin monomer and the barbed end, the value of which, resulting from the fitting procedure, is $\tau_+ = \frac{1}{k_+ c} \approx 10^{-3}$s for a typical actin concentration of $c \approx \mu$M. This hierarchy of the characteristic times guarantees an apparently linear dependence of the polymerization rate on the actin concentration, as required by the experimental results. At the same time, the results of the model are insensitive to the exact value of τ_{diff} as long as the requirement $\tau_+ \gg \tau_{\text{diff}}$ is fulfilled.

Second, we assume that the rate constants for formation and disruption of the preliminary bond, k_+, k_-, and the preliminary bond energy, U_{AA}^{prel}, are unaffected by formin. This assumption has a partial support based on the experimental evidence that formin does not influence the critical concentration of actin polymerization c^*, which is expressed as a combination of these three parameters (Eq. 11).

Lastly, the energies associated with the intermediate stages of the polymerization cycle are assumed to be linear functions of the reaction coordinates, signifying that the energies are accumulated or released in a constant gradual fashion. Investigation of nonlinear energy functions (not shown) indicates that if they represent high energy barriers, the polymerization rates of the formin-capped filaments are always lower than those of uncapped ones. On the other hand, certain nonlinear shapes of these functions result in even larger acceleration of polymerization than those described above. The polymerization rate can reach up to 15–20 times the elongation rate on uncapped filaments. However, it is unclear what physical mechanism could be associated with such energy profiles.

APPENDIX: ANALYTICAL RESULTS

In the following, the energy functions u_F and u_{AA} are expressed in units of k_BT.

Uncapped filaments

Solution of Eq. 9 under steady-state conditions gives for the probability distribution

$$\rho_A(z) = e^{-u_{AA}(z)}\left(\rho_A(0) - \frac{J_A}{D_A}\int_0^z e^{u_{AA}(t)}dt\right), \qquad (A1)$$

where $\rho_A(0)$ can be found from the normalization condition

$$\int_0^{z_0}\rho_A(z) = 1 \qquad (A2)$$

and the probability flux J_A, which determines the polymerization rate, $J_A = R_{AA}$, follows from simultaneous solution of Eqs. 8, A1, and A2,

$$R_{AA} = \frac{\frac{k_+c}{k_-}e^{u_{AA}(0)-u_{AA}(y_0)} - 1}{e^{u_{AA}(0)}\left(\frac{1}{k_-} + \frac{k_+c}{k_-}\frac{e^{-u_{AA}(z_0)}}{D_A}\int_0^{z_0}e^{u_{AA}(z)}dz\right)\int_0^{z_0}e^{-u_{AA}(z)}dz + \frac{1}{D_A}\left(1 - \frac{k_+c}{k_-}e^{u_{AA}(0)-u_{AA}(z_0)}\right)\int_0^{z_0}e^{-u_{AA}(z)}\int_0^z e^{-u_{AA}(\zeta)}d\zeta dz}. \qquad (A3)$$

The corresponding elongation slope defined in the main text is given by

$$\alpha_{AA} = \frac{\frac{k_+}{k_-}e^{u_{AA}(0)-u_{AA}(y_0)}}{\frac{e^{u_{AA}(0)}}{k_-}\int_0^{z_0}e^{-u_{AA}(z)}dz + \frac{1}{D_A}\int_0^{z_0}e^{-u_{AA}(z)}\int_0^z e^{-u_{AA}(\zeta)}d\zeta}. \qquad (A4)$$

For linear energy function $u_{AA}(z)$, the expression Eq. A4 for the elongation slope is reduced to

$$\alpha_{AA} = \frac{\frac{k_+}{k_-}e^{-U_{AA}}}{\frac{z_0}{k_-}\frac{1-e^{-U_{AA}}}{U_{AA}} + \frac{z_0^2}{D_A}\left(\frac{U_{AA}+e^{U_{AA}}-1}{U_{AA}^2}\right)}. \qquad (A5)$$

Based on the experimentally measured value of the elongation slope of uncapped actin, α_{AA}^{exp}, the relationship between k_+ and U_{AA} is

$$k_+^{fit} = \frac{\alpha_{AA}^{exp}z_0U_{AA}(e^{U_{AA}}-1)}{\alpha_{AA}^{exp}\frac{z_0^2}{D_A}c^*(1-U_{AA}-e^{-U_{AA}}) + U_{AA}^2}. \qquad (A6)$$

Formin-capped filaments

The probability distributions for the states corresponding to the two subprocesses follow from solutions of Eqs. 3–7 and are given by

$$\rho_E(x) = e^{-u_F(x)}\left(\rho_E(0) + \frac{J_E}{D_E}\int_0^x e^{u_F(t)}dt\right), \qquad (A7)$$

$$\rho_L(y) = e^{-u_F(y)-u_{AA}(y)}\left(\rho_L(0) - \frac{J_L}{D_L}\int_0^y e^{-u_E(t)+u_{AA}(t)}dt\right), \qquad (A8)$$

where the integration constants $\rho_L(0)$, $\rho_E(0)$ can be found from the normalization condition

$$\int_0^{y_0}\rho_L(y)dy + \int_0^{x_0}\rho_E(x)dx = 1 \qquad (A9)$$

and the probability fluxes determining the elongation rate in the steady-state regime $J_E = J_L = R_{AF}$ are

$$R_{AF} = \frac{\frac{k_+c}{k_-}e^{u_L(0)-u_L(y_0)} - e^{u_E(0)-u_E(x_0)}}{M},$$

$$M = \left(\frac{e^{-u_F(x_0)}\int_0^{x_0}e^{u_F(x)}dx}{D_E} + \frac{e^{-u_F(y_0)-u_{AA}(y_0)}}{D_L}\int_0^{y_0}e^{u_F(\zeta)+u_{AA}(\zeta)}d\zeta\right)\times\left(e^{u_F(0)}\int_0^{x_0}e^{-u_F(x)}dx + \frac{k_+c}{k_-}e^{u_F(0)+u_{AA}(0)}\int_0^{y_0}e^{-u_F(\zeta)-u_{AA}(\zeta)}d\zeta\right) + \ldots$$
$$+\frac{k_+c}{k_-}e^{u_F(0)+u_{AA}(0)-u_F(y_0)+u_{AA}(y_0)}\left(\frac{\int_0^{x_0}e^{u_F(x)}\int_0^x e^{-u_F(\zeta)}d\zeta dx}{D_E} - \frac{\int_0^{y_0}e^{u_F(\chi)+u_{AA}(\chi)}\int_0^x e^{-u_F(\zeta)-u_{AA}(\zeta)}d\zeta d\chi}{D_L} - \frac{e^{u_F(0)+u_{AA}(0)}}{k_-}\int_0^{y_0}e^{u_F(\zeta)+u_{AA}(\zeta)}d\zeta\right)$$
$$-e^{u_F(0)-u_F(x_0)}\left(\frac{\int_0^{x_0}e^{u_F(x)}\int_0^x -u_F(\zeta)d\zeta dx}{D_E} - \frac{\int_0^{y_0}e^{u_F(\chi)+u_{AA}(\chi)}\int_0^x -u_F(\zeta)-u_{AA}(\zeta)d\zeta d\chi}{D_L} - \frac{e^{u_F(0)+u_{AA}(\zeta)}}{k_-}\int_0^{y_0}e^{-u_F(\zeta)-u_{AA}(\zeta)}d\zeta\right). \qquad (A10)$$

For the linear forms for the potential functions $u_F(\zeta)$and $u_{AA}(\zeta)$, the elongation slope is

$$\alpha_{AF} = \frac{\frac{k_+}{k_-}e^{-U_{AA}}}{\frac{y_0^2}{D_L}\left[\frac{(1-e^{-U_{AA}-U_F})(1-e^{-U_F})}{U_F(U_F+U_{AA})}\frac{x_0}{y_0} + \frac{U_F+U_{AA}+e^{-U_{AA}-U_F}-1}{(U_F+U_{AA})^2}\right] + \frac{x_0^2}{D_E}\left(\frac{e^{-2U_F}-3e^{-U_F}+2-U_F}{U_F^2}\right) + \frac{e^{-U_{AA}-U_F}}{k_-}\left(\frac{1-e^{-U_F}}{U_F}x_0 + \frac{e^{U_F+U_{AA}}-1}{U_F+U_{AA}}y_0\right)}. \qquad (A11)$$

Inserting the relationship Eq. A6 for k_+, we obtain for the elongation slope

$$\alpha_{AF} = \frac{1}{\frac{y_0^2 c^*}{D_L}\left[\frac{(1-e^{-U_{AA}-U_F})(1-e^{-U_F})}{U_F(U_F+U_{AA})}\frac{x_0}{y_0} + \frac{U_F+U_{AA}+e^{-U_{AA}-U_F}-1}{(U_F+U_{AA})^2}\right] + \frac{x_0^2 c^*}{D_E}\left(\frac{e^{-2U_F}-3e^{-U_F}+2-U_F}{U_F^2}\right) + \frac{e^{-U_F}}{k_+^{fit}}\left(\frac{1-e^{-U_F}}{U_F}x_0 + \frac{e^{U_F+U_{AA}}-1}{U_F+U_{AA}}y_0\right)}. \quad \text{(A12)}$$

We are grateful to Alexander Bershadsky, David Kovar, Alexander Mogilner, Thomas Pollard, and Michael Rosen for discussions.

The financial support for M.M.K. by Israel Science Foundation, United States-Israel Binational Science Foundation, and the Marie Curie Network ''Flippases'' is gratefully acknowledged.

REFERENCES

1. Higgs, H. N. 2005. Formin proteins: a domain-based approach. *Trends Biochem. Sci.* 30:342–353.
2. Kovar, D. R. 2006. Molecular details of formin-mediated actin assembly. *Curr. Opin. Cell Biol.* 18:11–17.
3. Pollard, T. D. 2004. Formins coming into focus. *Dev. Cell.* 6:312–314.
4. Wallar, B. J., and A. S. Alberts. 2003. The formins: active scaffolds that remodel the cytoskeleton. *Trends Cell Biol.* 13:435–446.
5. Watanabe, N., and C. Higashida. 2004. Formins: processive cappers of growing actin filaments. *Exp. Cell Res.* 301:16–22.
6. Zigmond, S. H. 2004. Formin-induced nucleation of actin filaments. *Curr. Opin. Cell Biol.* 16:99–105.
7. Chang, F., D. Drubin, and P. Nurse. 1997. Cdc12p, a protein required for cytokinesis in fission yeast, is a component of the cell division ring and interacts with profilin. *J. Cell Biol.* 137:169–182.
8. Evangelista, M., D. Pruyne, D. C. Amberg, C. Boone, and A. Bretscher. 2002. Formins direct Arp2/3-independent actin filament assembly to polarize cell growth in yeast. *Nat. Cell Biol.* 4:260–269.
9. Feierbach, B., and F. Chang. 2001. Roles of the fission yeast formin for3p in cell polarity, actin cable formation and symmetric cell division. *Curr. Biol.* 11:1656–1665.
10. Kobielak, A., H. A. Pasolli, and E. Fuchs. 2004. Mammalian formin-1 participates in adherens junctions and polymerization of linear actin cables. *Nat. Cell Biol.* 6:21–30.
11. Pellegrin, S., and H. Mellor. 2005. The Rho family GTPase RIF induces filopodia through mDia2. *Curr. Biol.* 15:129–133.
12. Sagot, I., S. K. Klee, and D. Pellman. 2002. Yeast formins regulate cell polarity by controlling the assembly of actin cables. *Nat. Cell Biol.* 4: 42–50.
13. Schirenbeck, A., T. Bretschneider, R. Arasada, M. Schleicher, and J. Faix. 2005. The diaphanous-related formin dDia2 is required for the formation and maintenance of filopodia. *Nat. Cell Biol.* 7: 619–625.
14. Severson, A. F., D. L. Baillie, and B. Bowerman. 2002. A formin homology protein and a profilin are required for cytokinesis and Arp2/3-independent assembly of cortical microfilaments in *C. elegans*. *Curr. Biol.* 12:2066–2075.
15. Butler, B., C. Gao, A. T. Mersich, and S. D. Blystone. 2006. Purified integrin adhesion complexes exhibit actin-polymerization activity. *Curr. Biol.* 16:242–251.
16. Riveline, D., E. Zamir, N. Q. Balaban, U. S. Schwarz, T. Ishizaki, S. Narumiya, Z. Kam, B. Geiger, and A. D. Bershadsky. 2001. Focal contacts as mechanosensors: externally applied local mechanical force induces growth of focal contacts by an mDia1-dependent and ROCK-independent mechanism. *J. Cell Biol.* 153:1175–1186.
17. Pruyne, D., M. Evangelista, C. Yang, E. Bi, S. Zigmond, A. Bretscher, and C. Boone. 2002. Role of formins in actin assembly: nucleation and barbed-end association. *Science.* 297:612–615.
18. Zigmond, S. H., M. Evangelista, C. Boone, C. Yang, A. C. Dar, F. Sicheri, J. Forkey, and M. Pring. 2003. Formin leaky cap allows elongation in the presence of tight capping proteins. *Curr. Biol.* 13: 1820–1823.
19. Kovar, D. R., and T. D. Pollard. 2004. Insertional assembly of actin filament barbed ends in association with formins produces picoNewton forces. *Proc. Natl. Acad. Sci. USA.* 98:15009–15013.
20. Romero, S., C. Le Clainche, D. Didry, C. Egile, D. Pantaloni, and M. F. Carlier. 2004. Formin is a processive motor that requires profilin to accelerate actin assembly and associated ATP hydrolysis. *Cell.* 119: 419–429.
21. Vavylonis, D., D. R. Kovar, B. O'Shaughnessy, and T. D. Pollard. 2006. Model of formin-associated actin filament elongation. *Mol. Cell.* 21:455–466.
22. Kovar, D. R., J. Q. Wu, and T. D. Pollard. 2005. Profilin-mediated competition between capping protein and formin Cdc12p during cytokinesis in fission yeast. *Mol. Biol. Cell.* 16:2313–2324.
23. Pring, M., M. Evangelista, C. Boone, C. Yang, and S. H. Zigmond. 2003. Mechanism of formin-induced nucleation of actin filaments. *Biochemistry.* 42:486–496.
24. Kozlov, M. M., and A. D. Bershadsky. 2004. Processive capping by formin suggests a force-driven mechanism of actin polymerization. *J. Cell Biol.* 167:1011–1017.
25. Kovar, D. R., E. S. Harris, R. Mahaffy, H. N. Higgs, and T. D. Pollard. 2006. Control of the assembly of ATP- and ADP-actin by formins and profilin. *Cell.* 124:423–435.
26. Otomo, T., D. R. Tomchick, C. Otomo, S. C. Panchal, M. Machius, and M. K. Rosen. 2005. Structural basis of actin filament nucleation and processive capping by a formin homology 2 domain. *Nature.* 433: 488–494.
27. Shemesh, T., T. Otomo, M. K. Rosen, A. D. Bershadsky, and M. M. Kozlov. 2005. A novel mechanism of actin filament processive capping by formin: solution of the rotation paradox. *J. Cell Biol.* 170: 889–893.
28. Xing, J., H. Wang, and G. Oster. 2005. From continuum Fokker-Planck models to discrete kinetic models. *Biophys. J.* 89:1551–1563.
29. Kasai, M., and F. Oosawa. 1969. Behavior of divalent cations and nucleotides bound to F-actin. *Biochim. Biophys. Acta.* 172:300–310.
30. Zimmerle, C. T., and C. Frieden. 1986. Effect of temperature on the mechanism of actin polymerization. *Biochemistry.* 25:6432–6438.
31. Kuhn, J. R., and T. D. Pollard. 2005. Real-time measurements of actin filament polymerization by total internal reflection fluorescence microscopy. *Biophys. J.* 88:1387–1402.
32. Pollard, T. D., and G. G. Borisy. 2003. Cellular motility driven by assembly and disassembly of actin filaments. *Cell.* 112:453–465.